

# Enhancement of the second-harmonic generation based on the cascaded second- and third-order nonlinear processes in a multimode optical microcavity

Ming Li,<sup>1</sup> Chang-Ling Zou,<sup>2,\*</sup> Chun-Hua Dong,<sup>2</sup> Xi-Feng Ren,<sup>2</sup> and Dao-Xin Dai<sup>1,†</sup>

<sup>1</sup>*Centre for Optical and Electromagnetic Research, JORCEP,  
State Key Laboratory for Modern Optical Instrumentation,*

*Zhejiang Provincial Key Laboratory for Sensing Technologies, Zhejiang University, Hangzhou 310058, China*

<sup>2</sup>*Key Laboratory of Quantum Information, CAS,  
University of Science and Technology of China, Hefei 230026, China*

Optical microcavities are often used to realize enhanced nonlinear optical interactions for highly efficient second-harmonic generation. With increased pump power, the efficiency of nonlinear frequency conversion can be increased further, while some other unwanted nonlinear effects will also emerge, leading to complicated dynamics or instability. Here, we study the interplay between cascaded second- and third-order nonlinear processes and investigate their impact on the second-harmonic generation in microcavities. It is found that the non-degenerate optical parametric oscillation (OPO) appears and the presence of  $\chi^{(3)}$  process can modify the OPO threshold significantly when the multimode cavity is strongly pumped at the fundamental optical mode. One can even break the efficiency limitation of the second-harmonic mode restricted by the OPO by utilizing the interference between the OPO and the four-wave mixing. The present coherent interplay between nonlinear optical processes in microcavities is conducive to exploring new physics in the cavity nonlinear photonics.

PACS numbers: 42.65.k, 42.82.m, 42.65.Ky

## I. INTRODUCTION

Cavity-assisted nonlinear optical effects have been studied since the last century for their applications in parametric amplification [1], frequency conversion [2, 3] and frequency combs [4], by putting nonlinear crystals in traditional macroscopic Fabry-Perot or ring-type cavities. Along with the development of fabrication technologies for high- $Q$  microcavities [5–7], strong nonlinear optical effects have been demonstrated [6, 8, 9], in which the nonlinear interaction between photons of different colors is greatly enhanced due to the small mode volume of microcavities. Enhanced nonlinear photonics in microcavities enables low-threshold lasers [10, 11], optical parametric oscillators [12], optical squeezing [13, 14], frequency combs [15–20], spontaneous down-conversion quantum photon sources [21–25], highly efficient frequency conversion [26–28] as well as second-harmonic and third-harmonic generation [29–36].

As has been demonstrated in the previous researches, different nonlinear processes might happen simultaneously in an optical microcavity [9, 37, 38]. For example, parametric down-conversion can be observed along with the second-harmonic generation (SHG) [39]. This type of cascaded second-order ( $\chi^{(2)}$ ) nonlinear processes have been studied a lot in both classical and quantum fields [40, 41]. By harnessing the cascaded effect of the  $\chi^{(2)}$  nonlinearity, it is feasible to achieve efficient higher-order harmonic light generation [32, 37, 39, 42], multipartite entanglement [43] and frequency combs in different mode families [44–46]. However, for the analysis of those

nonlinear optical processes, previously people usually use a simple model, in which only the  $\chi^{(2)}$  nonlinearity is taken into consideration. Such a simple model is only valid when the other nonlinear interactions such as  $\chi^{(3)}$  and Raman are very weak, or the interactions involving other modes are not on-resonance [35]. In presence of the  $\chi^{(3)}$ , Raman or other types of nonlinear processes, the  $\chi^{(2)}$  nonlinear process may be affected. As a result, the simple model does not work well.

For example, for the SHG, the high SH power will dissipate to other modes through spontaneous down-conversion, and the pump power may also be dissipated to other modes through the spontaneous four-wave mixing (FWM). As a result, the high conversion efficiency predicted by the simple model may be invalid. A fundamental question for the multimode cavity nonlinear photonic system is: what is the efficiency of SHG in a cavity supporting both  $\chi^{(2)}$  and  $\chi^{(3)}$  nonlinearity and will the different nonlinear processes interfere with each other? In this work, we establish an improved model containing both the  $\chi^{(2)}$  and  $\chi^{(3)}$  nonlinear interactions in a multimode microcavity. With this model, we investigate the interference between cascaded second-order process and third-order process and its effect on SHG. According to our calculations, the  $\chi^{(3)}$  process can modify the threshold of parametric down-conversion, thus altering the energy flow from the second-harmonic (SH) mode to its neighbor modes. It is revealed that a key for achieving higher SHG efficiency is to optimize the resonant frequency of the SH mode according to the coupling strength of the  $\chi^{(3)}$  process.

\* clzou321@ustc.edu.cn

† dxdai@zju.edu.cn

## II. INTERFERENCE BETWEEN $\chi^{(2)}$ AND $\chi^{(3)}$ PROCESSES

Fig.1(a) shows the considered microcavity system, where multiple optical modes in both the visible and infrared bands are supported in the same cavity. When the cavity is designed carefully for phase matching and tuned precisely for double resonances, efficient SHG can be achieved, as demonstrated experimentally in [35]. The photon interaction Hamiltonian is described by a  $\chi^{(2)}$  process between mode  $a$  and  $d$  as  $a^2d^\dagger + a^\dagger 2d$ . Traditionally, most work in cavity-enhanced SHG was based on the double-resonance condition and the non-depletion approximation [30, 31, 33]. For the case with weak pump power and weak nonlinear effect, the spontaneous parametric down-conversion (SPDC) and FWM processes induced by the vacuum fluctuation can be neglected. Therefore, the SHG process is often approximately modeled as two coupled harmonic oscillators.

However, one should notice that there also exist multiple adjacent modes near mode  $a$  and  $d$  in a cavity. The orbit angular momentum of these modes differ by integers and their frequencies are almost equally spaced. When the pump power increases, the intra-cavity photon number arrives at the threshold of stimulated emission at mode  $a$  due to the degenerate parametric down conversion process  $a^2d^\dagger + a^\dagger 2d$  (a reversal process of SHG), breaking the non-depletion condition of SHG. Also,  $d$  can couple to the adjacent modes ( $b, c$ ) around the fundamental mode  $a$  (see Fig. 1(a)) through non-degenerate SPDC ( $bcd^\dagger + b^\dagger c^\dagger d$ ). Both processes might decrease the efficiency of SHG.

In addition to the cascaded SHG and down-conversion, the  $\chi^{(3)}$  process redistributes the energy in the modes adjacent to  $a$  and  $d$  through the FWM. Taking the FWM, self-phase modulation (SPM) and cross-phase modulation (XPM) into consideration, the system can be described by the Hamiltonian [47],

$$H = \sum_0^{N_1} \omega_{f,j} f_j^\dagger f_j + \sum_0^{N_2} \omega_{s,j} s_j^\dagger s_j$$

$$H_{\chi^{(2)}} + H_{\chi^{(3)}}, \quad (1)$$

where  $f_j$  is the  $j$ -th mode in the fundamental mode family,  $s_j$  is the  $j$ -th mode in the SH mode family,  $H_{\chi^{(2)}} = \sum_{j,k,l} g_2^{jkl} (f_j f_k s_l^\dagger + f_j^\dagger f_k^\dagger s_l)$  is the interaction due to  $\chi^2$ ,  $H_{\chi^{(3)}}$  is the interaction due to  $\chi^3$  including the four-wave mixing in one mode family and between two mode families, which has the form  $g_3^{jklm} (f_j f_k s_l^\dagger s_m^\dagger + s_j s_k f_l^\dagger f_m^\dagger)$ .  $\omega_{f,j}$  is the resonant frequency of the  $j$ -th mode in the fundamental mode family and similar for the SH mode,  $N_1$  and  $N_2$  are the number of modes in each mode family,  $g_3$  and  $g_2$  represent the single photon coupling strength of the third- and second-order process.

In order to quantitatively analyze the system, we estimate the single photon coupling strengths of different processes. In a ring-type microcavity, the single photon coupling strength can be derived from the nonlinear interaction Hamiltonian  $E \cdot P_{nl}$ , which are given in

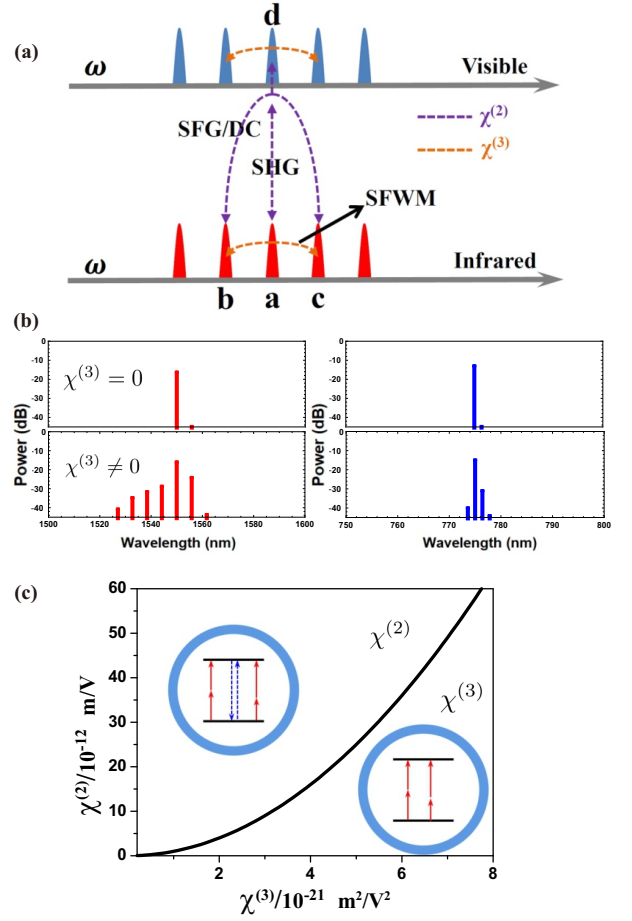


FIG. 1. (a) Schematic picture of hybrid nonlinear processes in a cavity. FWM: Four-wave mixing between  $a$  and  $b, c$ . SHG: Second-harmonic generation between  $a$  and  $d$ . SFG/DC: Sum-frequency generation/down conversion between  $d$  and  $b, c$ . (b) Simulated energy distribution in two mode families. Both cases are obtained by scanning the detuning of the two mode families. For the case  $\chi^{(3)} = 0$ , the system stays below the OPO threshold for all detunings. While  $\chi^{(3)}$  nonlinearity pushes the system above threshold. (c) Comparison between the coupling strengths of cascaded  $\chi^{(2)}$ - $\chi^{(2)}$  and  $\chi^{(3)}$  processes. Here we set  $\frac{3}{8\epsilon} \frac{\xi_2^2}{\xi_3} = 2.5 \times 10^{-2}$ ,  $\omega_1/2\pi = 2 \times 10^{14}$  Hz. The two processes will interfere with each other around the black line with  $Q = 10^5$ . For higher quality factors, the  $\chi^{(2)}$  process dominates. The insets are the energy diagram of cascaded  $\chi^{(2)}$ - $\chi^{(2)}$  process (up) and  $\chi^{(3)}$  process (down).

the following for SHG ( $\chi^{(2)}$ ) and degenerate FWM ( $\chi^{(3)}$ ) [8, 35],

$$hg_2 = \sqrt{\frac{\hbar\omega_1\hbar\omega_1\hbar\omega_2}{\epsilon_0\epsilon_1^2\epsilon_2}} \frac{3\chi^{(2)}}{4\sqrt{2}} \frac{1}{\sqrt{2\pi R}} \frac{1}{\sqrt{A_{eff}}} \xi_2 \quad (2)$$

$$hg_3 = \sqrt{\frac{(\hbar\omega_1)^2\hbar\omega_2\hbar\omega_3}{(\epsilon_0\epsilon_2)^2\epsilon_1\epsilon_3}} \chi^{(3)} \frac{3}{2} \frac{1}{2\pi R} \frac{1}{A_{eff}} \xi_3 \quad (3)$$

where  $R$  is the radius of the microcavity,  $\xi_i$  is the mode overlap factor in the cross section and fulfills  $0 \leq \xi_i \leq 1$ ,

$A_{eff}$  is the effective mode area in the cross section,  $\epsilon_i$  is the relative dielectric constant at frequency  $\omega_i$ .

To give a preliminary proof of the complicated multimode and multiple nonlinearity processes, we numerically simulate the coupling between the 1550 nm fundamental frequency mode family (30 modes) and 775 nm SH mode family (30 modes) in a AlN microcavity based the Hamiltonian in Equation (1). The parameters used in the simulation are  $g_2 = 0.1$  MHz,  $g_3 = 5$  Hz,  $D_1^{1550} = 4.57 \times 10^{12}$  Hz,  $D_2^{1550} = 1.76 \times 10^9$  Hz,  $D_1^{775} = 4.42 \times 10^{12}$  Hz,  $D_2^{775} = 2.06 \times 10^9$  Hz, where the dispersive parameter  $D_1$  and  $D_2$  are derived from the Taylor expansion of the resonance frequency  $\omega_j = \omega_0 + jD_1 + \frac{1}{2!}D_2 + \dots$ . These parameters are referred to the experimental work in Ref.[47]. As shown in Fig. 1(b), without the  $\chi^{(3)}$  interaction, there are only two modes generated and the system operates below the OPO threshold (the critical point that the adjacent modes just start to oscillate). When there exists the  $\chi^{(3)}$  interaction, OPO appears and many modes are excited in each mode family. As a result, the energy flows to mode  $b, c$  and their adjacencies, and the SHG efficiency decreases. The preliminary analysis shows that the  $\chi^{(2)}$  process is indeed influenced by the  $\chi^{(3)}$  process.

Considering that the visible modes have lower  $Q$  and the pump is in the infrared band, it is reasonable to neglect the FWM in the visible band. Due to the dispersion of the cavity mode, resonant modes far from the pump have relatively large detunings. This is also verified by the results in Fig. 1(b) that only a few of modes near  $d$  in the visible band is significantly involved in the nonlinear processes. Therefore, there are mainly three processes in the microcavity:

- (i)  $\chi^{(2)}$  process ( $a + a \rightarrow d$ ), with a coupling strength  $g_2$ .
- (ii)  $\chi^{(3)}$  process ( $a + a \rightarrow b + c$ ) with a coupling strength  $g_3$ .
- (iii) cascaded  $\chi^{(2)}$ - $\chi^{(2)}$  process ( $a + a \rightarrow d \rightarrow b + c$ ) [40]. The effective coupling strength scales with  $g_2^2/(-i\delta_d - \kappa_d)$ , where  $\delta_d$  and  $\kappa_d$  are the detuning and decay rate of mode  $d$ , respectively.

Generally, the  $\chi^{(3)}$  susceptibility of non-centrosymmetric materials is 8 to 10 order of magnitude smaller than  $\chi^{(2)}$  [48]. The third-order nonlinear interaction of optical modes is negligible compared to second-order interaction for most situations in traditional bulk, fiber and waveguide optics. Things may change when we study the nonlinear interaction in an optical cavity. The highly concentrated optical field in both space and time domain will significantly enhance the interaction strengths in different manners for different processes. The processes (ii) and (iii) are negligible for small pump power, and should be taken into consideration when the effective cooperativity  $C^{(ii)} = g_3^2 N_a^2 / \kappa_b \kappa_c$  and  $C^{(iii)} = g_2^2 N_d / \kappa_b \kappa_c$  approach unity, where  $N_d \lesssim 4g_2^2 N_a^2 / \kappa_d^2$ ,  $\kappa_i$  is the decay rate of the  $i$ -th mode with  $i \in \{a, b, c, d\}$ . Under certain conditions, the probability amplitudes of these processes might have the same order of magnitude. The phase between

the two paths will cause constructive or destructive interference.

When the coupling strength  $g_3$  and  $g_2^2/\kappa_d$  are comparable, i.e.  $C^{(ii)} \sim C^{(iii)}$ , the interference of the three nonlinear processes occurs if the pump (or intracavity photon number  $N_a$  in the pump mode) is large enough. This condition requires

$$\kappa_d \simeq \frac{g_2^2}{g_3} \simeq \frac{3\omega_1 \xi_2^2 \chi^{(2)2}}{8\epsilon \xi_3 \chi^{(3)}}. \quad (4)$$

Generally, the  $\chi^{(2)}$  and  $\chi^{(3)}$  susceptibility are at the order of  $10^{-12} \text{m/V}$  and  $10^{-21} \text{m}^2/\text{V}^2$ , respectively. Thus the value of  $\kappa_d \simeq g_2^2/g_3$  should be of the magnitude of  $10^9 \sim 10^{10}$  Hz, corresponding to cavity quality factor  $Q$  of the magnitude  $10^4 \sim 10^5$  at telecommunication wavelength. This condition is realistic for many integrated photonic platform, such as Aluminum Nitride (AlN) [26, 35], GaAs [49], GaN [50] and Lithium Niobate (LN) [51, 52]. Note that the condition can be relaxed by changing the detuning of mode  $d$  or engineering the mode overlap factors. In Fig. 1(c), we plot the scaling relation between the coupling strengths of the cascaded  $\chi^{(2)}$ - $\chi^{(2)}$  process and  $\chi^{(3)}$  process. The black line shows the situation that the coupling strength  $g_2^2/\kappa_d$  of the cascaded  $\chi^{(2)}$ - $\chi^{(2)}$  process equals  $g_3$ . From this figure, it can be seen that the coupling strength  $g_3$  of the third-order process possibly becomes comparable to or even higher than the cascaded second-order process, which depends on the detuning and quality factor of mode  $d$ . When  $g_3 > g_2^2/\kappa_d$  (i.e., the upper area of Fig. 1(c)), the cascaded  $\chi^{(2)}$ - $\chi^{(2)}$  process is dominant in the system.

### III. MODEL

In this section, we study the simplified model that only includes the nearest modes  $b, c$ , to simplify the complex nonlinear system and reveal the essential physics of the multimode and multiple nonlinear processes. In presence of continuous-wave pumping field with frequency near mode  $a$ , the Hamiltonian can be written as

$$H = \omega_{a,0} a^\dagger a + \omega_{b,0} b^\dagger b + \omega_{c,0} c^\dagger c + \omega_{d,0} d^\dagger d + g_3(a^\dagger b c + a^2 b^\dagger c^\dagger) + g_{22}(a^\dagger d + a^2 d^\dagger) + g_{21}(bcd^\dagger + b^\dagger c^\dagger d) + \epsilon_a(ae^{i\omega_a t} + a^\dagger e^{-i\omega_a t}). \quad (5)$$

Here,  $\omega_{x,0}$  is the resonant frequency of the mode  $x$  with  $x \in \{a, b, c, d\}$ ,  $\omega_a$  is the pump frequency near the resonance of mode  $a$ ,  $g_3$ ,  $g_{22}$  and  $g_{21}$  represent the single photon coupling strength of FWM, SHG and sum-frequency generation.  $\epsilon_a = \sqrt{\frac{2\kappa_{a,1} P_a}{\hbar\omega_a}}$  is the pump field strength,  $\kappa_{a,1}$  is the external coupling rate between cavity and waveguide and  $P_a$  is the pump power to mode  $a$ . Note that the Hamiltonian does not contain self-phase modulation (SPM) and cross-phase modulation (XPM) terms, which only shift the frequencies of the resonant modes in our case. Here, we only care about the steady

state behavior of the system. In the rotating frame, the Hamiltonian can be simplified to,

$$\begin{aligned}
H = & \delta_a a^\dagger a + \delta_b b^\dagger b + \delta_c c^\dagger c + \delta_d d^\dagger d \\
& + g_3(a^\dagger b c + a^2 b^\dagger c^\dagger) + g_{21}(d^\dagger b c + d b^\dagger c^\dagger) \quad (6) \\
& + g_{22}(a^\dagger d + a^2 d^\dagger) + \epsilon_a(a + a^\dagger)
\end{aligned}$$

where  $\delta_x = \omega_{x,0} - \omega_a$  with  $x \in \{a, b, c\}$  and  $\delta_d = \omega_{d,0} - 2\omega_a$ .

For pump power below the OPO threshold  $P < P_c$ ,  $b = c = 0$  (neglecting the vacuum induced SPDC and FWM), the Hamiltonian reduces to the form of simple two-mode SHG. Now we consider the pump power  $P > P_c$ , under which the energy might flow to mode  $b$  and  $c$  with  $b, c \neq 0$ . Following the Heisenberg equation and mean field approximation [26, 35], the dynamics of the operator and the corresponding mean field of each mode both obey the following form,

$$\frac{d}{dt}b = (-i\delta_b - \kappa_b)b - ig_3a^2c^\dagger - ig_{21}c^\dagger d \quad (7)$$

$$\frac{d}{dt}a = (-i\delta_a - \kappa_a)a - i2g_3a^\dagger bc - i2g_{22}a^\dagger d - i\epsilon_a \quad (8)$$

$$\frac{d}{dt}c = (-i\delta_c - \kappa_c)c - ig_3a^2b^\dagger - ig_{21}b^\dagger d \quad (9)$$

$$\frac{d}{dt}d = (-i\delta_d - \kappa_d)d - ig_{22}a^2 - ig_{21}bc. \quad (10)$$

Here, we neglect the fluctuations and only concern the mean field of each mode. The amplitudes of the fields are treated as complex numbers. At steady state,  $\frac{do}{dt} = 0$  with  $o \in \{a, b, c, d\}$ , and we get four coupled nonlinear equations. Multiplying Eq. (7) by the conjugate of Eq. (9), we get the pump independent parameter

$$|g_3a_s^2 + g_{21}d_s|^2 = |(-i\delta_b - \kappa_b)(i\delta_c - \kappa_c)|, \quad (11)$$

where  $a_s$  and  $d_s$  are the amplitude of the fundamental and SH mode at steady state. The parameter depends only on the detunings and decay rates of mode  $b, c$ , which is similar to the OPO threshold [53]. In absence of the  $\chi^{(3)}$  process, the maximum intracavity SH light amplitude fulfills the threshold relation

$$|g_{21}d_s|^2 = |(-i\delta_b - \kappa_b)(i\delta_c - \kappa_c)|. \quad (12)$$

Comparing equation 11 with 12, it is found that the interference between  $\chi^{(2)}$  and  $\chi^{(3)}$  process alters the steady state (maximum) value of  $|d_s|^2$  by the factor  $g_3a_s^2$ . We can imagine that opposite phases of  $g_3a_s^2$  and  $g_{21}d_s$  will give larger value of  $|d_s|$ , compared with the pure  $\chi^{(2)}$  process. In this sense, the  $\chi^{(3)}$  process increases the SHG power.

Before calculating the SHG efficiency, we first investigate the threshold of the OPO. The photons in mode  $a$  and  $d$  can both provide ‘‘gain’’ for  $b, c$  via nonlinear interactions. If the ‘‘gain’’ can compensate the decay of mode  $b, c$ , parametric oscillation in these modes appears. However, the ‘‘gain’’ from the two different paths have different phases, which may result in constructive or destructive interference of the cascaded  $\chi^{(2)}$ - $\chi^{(2)}$  and  $\chi^{(3)}$

processes. As a result, the effective ‘‘gain’’ determines the threshold of the system. For pump power below threshold,  $b = c = 0$ , the steady state intracavity photon numbers of  $a$  and  $d$  are related by SHG

$$d_s = \frac{ig_{22}}{-i\delta_d - \kappa_d}a_s^2. \quad (13)$$

Increasing the pump power to the threshold  $P_c$ , equation 11 and 13 hold simultaneously, we get

$$|g_3 + \frac{ig_{21}g_{22}}{-i\delta_d - \kappa_d}|^2|a_s|^4 = |(-i\delta_b - \kappa_b)(i\delta_c - \kappa_c)|.$$

We can further derive the intracavity photon number  $A_s$  in mode  $a$  at the threshold

$$A_s = |a_s|^2 = \frac{\sqrt{|(-i\delta_b - \kappa_b)(i\delta_c - \kappa_c)|}}{|g_3 + \frac{ig_{21}g_{22}}{-i\delta_d - \kappa_d}|} \quad (14)$$

and the pump threshold  $P_c$  of OPO

$$\begin{aligned}
P_c = & \frac{\hbar\omega_a}{2\kappa_{a,1}} \times \\
& \left( \frac{4g^4}{\delta_b^2 + \kappa_d^2} A_s^3 + 4g^2 \frac{\kappa_a\kappa_d - \delta_a\delta_d}{\delta_b^2 + \kappa_d^2} A_s^2 + (\delta_a^2 + \kappa_a^2) A_s \right). \quad (15)
\end{aligned}$$

Equation (14) indicates that the coupling strength  $g_3$  and cascaded parameter  $\frac{ig_{21}g_{22}}{-i\delta_d - \kappa_d}$  have different phases depending on the second-order coupling strengths  $g_{21}$  and  $g_{22}$ , the detuning and decay rate of mode  $d$ . As shown in Fig. 2(a), the threshold of pump power is altered by the detuning of the SH mode. For blue detuning of  $d$  ( $\delta_d > 0$ ) and  $g_3 > 0$ ,  $g_3$  and  $\frac{ig_{21}g_{22}}{-i\delta_d - \kappa_d}$  have opposite phases, resulting in destructive interference between the two processes. The destructive interference reduces the effective ‘‘gain’’ parameter, thus raising the threshold rapidly. For  $\delta_d = 2\kappa_d$ , the threshold increases by 26 times compared to the case  $g_3 = 0$ , and 16 times compared to OPO induced by only  $\chi^{(3)}$  process. While for red detuning, the two paths interfere constructively and can reduce the threshold (Fig. 2(a)), which may find application in building low-threshold parametric oscillators and frequency combs.

As a consequence, the generated SH power is changed in presence of  $\chi^{(3)}$  process in two ways. First, for the case  $g_3 = 0$ , the SH mode photon number has an upper bound  $\frac{|(-i\delta_b - \kappa_b)(i\delta_c - \kappa_c)|}{g_{21}^2}$  restricted by OPO threshold [40]. The change of the threshold promotes or reduces the upper bound. Second, even though Eq. (11) holds regardless of the pump power, the detuning  $\delta_d$  or the nonlinear coupling among the four modes may change the phase difference  $\Delta\theta$  between  $g_3a_s^2$  and  $g_{21}d_s$  to fulfill  $\pi/2 < \Delta\theta < 3\pi/2$ . In this case, the upper bound from OPO threshold can be broken if the pump is strong enough.

The relationship between the pump power and the output SH power is obtained by numerically solving the coupled nonlinear equations (Eqs. (7)-(10)) As shown in Fig. 3, one sees that the threshold changes for different

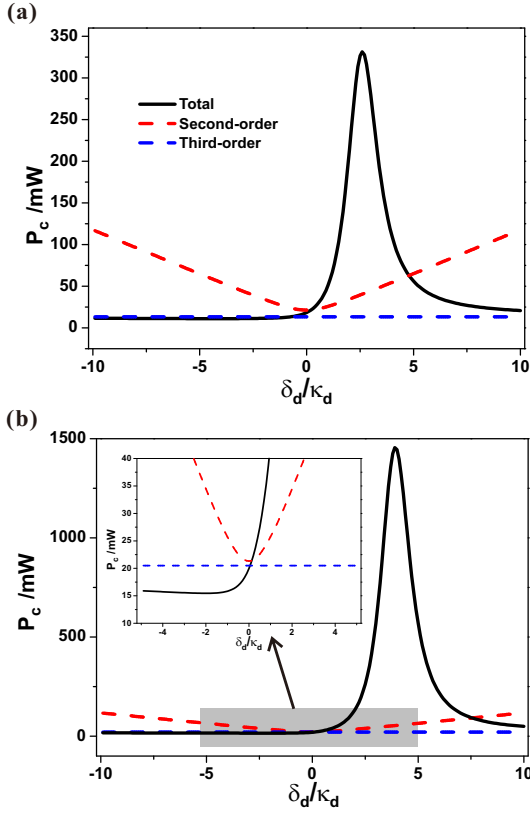


FIG. 2. Relation between the OPO threshold and detuning of the SH mode. (a) The parameters are  $g_3/2\pi = 10$  Hz,  $g_{22}/2\pi = 0.1 \times 10^6$  Hz,  $\kappa_d/2\pi = 0.8 \times 10^9$  Hz, which can be realized by the current fabrication technology in several platforms. The OPO threshold becomes much higher than both the thresholds induced by the  $\chi^{(3)}$  nonlinear process and cascaded  $\chi^{(2)}$ - $\chi^{(2)}$  process. (b) The case for  $g_3/2\pi = 6.5$  Hz. The inset shows the constructive interference of cascaded  $\chi^{(2)}$ - $\chi^{(2)}$  and  $\chi^{(3)}$  process for  $\delta_d < 0$ . Dashed Red: OPO threshold of cascaded  $\chi^{(2)}$ - $\chi^{(2)}$  process with  $g_3 = 0$ . Dashed Blue: threshold of  $\chi^{(3)}$  process with  $g_2 = 0$ . Black: threshold resulted from interference.

detunings, which is consistent with the results in Fig. 2. When the pump power increases beyond the threshold, part of the pump energy is converted to the neighbor modes of  $a$  and the SH power decreases. When destructive interference happens, the efficiency of the SHG can evolve along the isolated SHG curve to achieve a higher power, avoiding the energy flow to other modes in a large range of pump power. When constructive interference happens, the threshold is even lower than that of  $g_3 = 0$ , which accelerates the loss of pump energy. Another striking phenomenon we should pay attention is the conversion efficiency for pump powers above the threshold. The intra-cavity photon number of the SH mode is not restricted by the upper bound in general OPO process. Both the curves of destructive and constructive interference (Blue line in Fig. 3) can exceed the upper bound restricted by the general OPO (Solid red line in Fig. 3). Consequently, the SHG efficiency can be unambiguously increased by the interference effect. This phenomenon

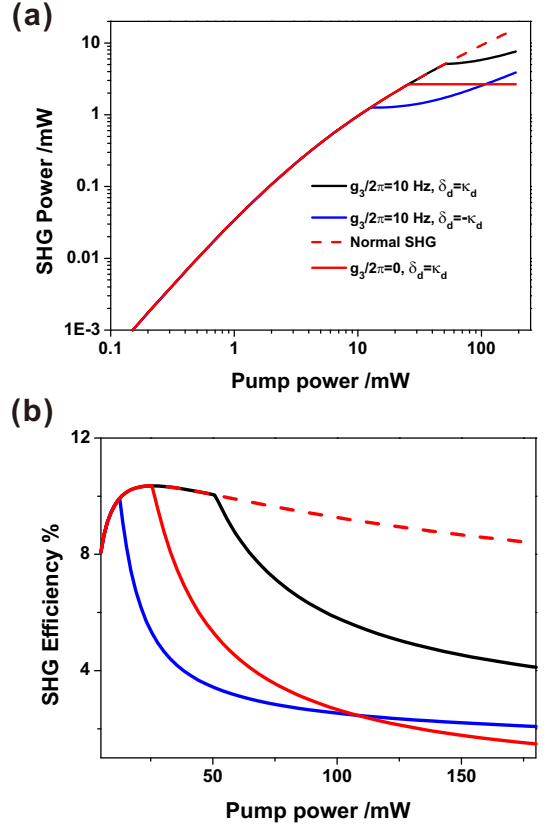


FIG. 3. Relation between the SH mode power (a), SHG efficiency (b) and the pump power. Dashed red: Isolated SHG; Solid Red: SHG with  $g_3 = 0$ . Black and Blue:  $g_3/2\pi = 10$  Hz, and  $\delta_d = \pm\kappa_d$ . Normal SHG: SHG only considering the coupling between the fundamental and SH mode.

indicates that the phase relation between  $g_3 a_s^2$  and  $g_{21} d_s$  can indeed change along with the increase of the pump, as well as the change of  $\delta_d$ . The photon number amplitude  $d_s$  in mode  $d$  must increase to compensate the increasing value of  $a_s^2$  to fulfill the conservation condition in equation 11. To summarize briefly, the interference can affect the SHG efficiency by changing the threshold of the system and breaking the restriction of OPO.

Then, we go further to investigate how to acquire higher SH power for any given pump power and micro-cavity. An effective way is to control the interference of different nonlinear processes to avoid or reduce the energy flow to the fundamental frequency modes near  $a$ . Changing the detuning of mode  $d$  to values having different signs with  $g_3$  can generate the desired destructive interference, which can be realized using thermal or electro-optic methods. Fig. 4 shows the intracavity photon number of the SH mode as the frequency detuning  $\delta_d$  varies. It can be seen that there is a strong correlation between the signs of  $g_3$  and  $\delta_d$ .

Since the detuning  $\delta_d$  between the SH mode and the frequency of pump laser can modify the phase relation of the two paths, it should be carefully controlled to improve the conversion efficiency. Note that zero detuning does not maximize the highest conversion efficiency. The

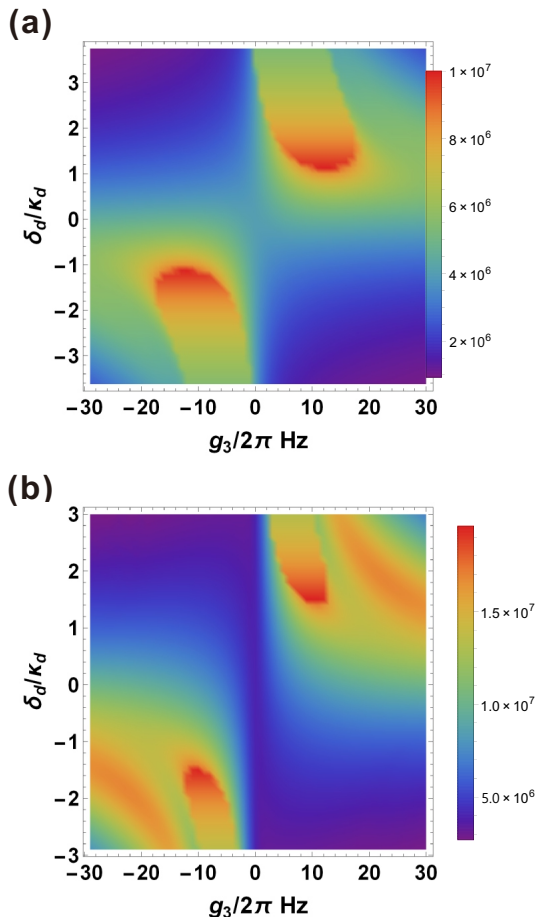


FIG. 4. Dependences of the intra-cavity photon number in the SH mode on the detuning  $\delta_d$  and the coupling strength  $g_3$  for different pump powers, with  $P = 70 \text{ mW}$  in (a) and  $P = 200 \text{ mW}$  in (b).

comparison between Figs. 4(a) and 4(b) indicates that the detuning for highest conversion efficiency is also related to the pump power, as well as  $g_3$ . This result demonstrates our deduction that the phase contrast of the two paths is intensity-dependent.

#### IV. DISCUSSION

Throughout our simulations, the second-order nonlinear coupling strength is  $g_2/2\pi = 0.1 \text{ Hz}$  and the third-order nonlinear coupling strength is at the order of  $1 - 10 \text{ Hz}$ . The decay rate of the SH mode is  $0.8 \times 10^9 \text{ Hz}$ , corresponding to loaded quality factor of  $2.5 \times 10^5$  at  $775 \text{ nm}$  wavelength. In Ref. [26, 35, 47], the authors reported AlN microrings with diameter of several tens of micrometer and measured the quality factor to be  $2.3 \times 10^5$  and  $1.16 \times 10^5$  in  $775 \text{ nm}$  and  $1550 \text{ nm}$  band. The estimated nonlinear coupling strengths are  $0.11 \text{ MHz}$  for second-order process and several  $\text{Hz}$  for third-order process. Since our simulation are based on the current fabrication technology, we believe our prediction could be experimentally realized in the near future.

In the above analysis, we have made several simplifications to the multimode microcavity with multiple nonlinear processes. The following processes are neglected: the FWM among the visible modes, SPM, XPM, sum/difference-frequency generation between the fundamental and SH modes. These simplifications are valid when the frequencies of the resonant modes are not equally spaced and the frequency shifts of the resonant modes due to SPM and XPM are small. For higher pump powers or microcavities with lower dispersion coefficients, more modes should be included to make a complete model. In addition, other nonlinear effects, such as Brillouin scattering, Raman scattering and nonlinear losses, may also play a significant role under certain conditions, which opens a new avenue for studying complex coherent nonlinear phenomenon in optical microcavities. In addition to the coherent interference between different nonlinear processes studied here, we think many other new phenomena will be observed experimentally in the near future. For example, as a reverse process of SHG, the  $\chi^{(2)}$ -assisted SPDC in microcavities can also be influenced by  $\chi^{(3)}$  nonlinearity. Another example is the third-harmonic generation, which can be realized via either  $\chi^{(3)}$  or cascaded  $\chi^{(2)}$ - $\chi^{(2)}$  nonlinear process. The coherent interference between different nonlinear processes provides a powerful method to engineer nonlinear photonics in a microcavity and develop new applications. In addition, the multiple mode microcavity with multiple nonlinear processes can also serve as a platform for fundamental studies on the dynamics and stabilities of complex nonlinear systems.

#### V. CONCLUSION

In conclusion, we have investigated the coherent interference between nonlinear  $\chi^{(3)}$  and cascaded  $\chi^{(2)}$ - $\chi^{(2)}$  processes in an optical cavity. For a multimode microcavity, the efficient SHG will accompany with the FWM at pump frequency and non-degeneration optical parametric oscillation generated by the SH light. We first demonstrate that the FWM and down-conversion can significantly affect the efficiency of SHG, due to the saturation and the conversion of the SH light to other modes. Then, we studied the coherent interplay between those nonlinear processes, and demonstrate that the interference can suppress the energy leakage from the SH mode to other modes. According to our analysis, the phase difference between the cascaded  $\chi^{(2)}$ - $\chi^{(2)}$  and  $\chi^{(3)}$  processes depends strongly on the detuning of the SH mode, which will significantly influence the threshold of the system. Above threshold, the upper bound of SHG efficiency for pure- $\chi^{(2)}$  nonlinearity can be broken for appropriate phase difference. Our study clearly explains the mechanism of SHG affected by other nonlinear processes and complements the blank in the study of SHG with high-power pump. It can be generalized to more complex systems containing many resonances which couple with each other via different nonlinear processes, including  $\chi^{(2)}$ ,



$\chi^{(3)}$  and high-order nonlinearities, as well as Raman and Brillouin scattering processes.

### ACKNOWLEDGMENTS

This work was supported by National Natural Science Foundation of China (NSFC) (61725503,

61431166001, 61505195, 61590932, 11774333), National Major Research and Development Program (No. 2016YFB0402502), Zhejiang Provincial Natural Science Foundation (Z18F050002), China Postdoctoral Science Foundation (NO. 2017M621919).

- 
- [1] J. Giordmaine and R. C. Miller, Tunable coherent parametric oscillation in  $LiNbO_3$  at optical frequencies, *Phys. Rev. Lett.* **14**, 973 (1965).
- [2] S. Pereira, M. Xiao, H. Kimble, and J. Hall, Generation of squeezed light by intracavity frequency doubling, *Phys. Rev. A* **38**, 4931 (1988).
- [3] Z. Ou, S. Pereira, E. Polzik, and H. J. Kimble, 85% efficiency for cw frequency doubling from 1.08 to 0.54  $\mu\text{m}$ , *Opt. Lett.* **17**, 640 (1992).
- [4] A. Bartels, D. Heinecke, and S. A. Diddams, 10-GHz self-referenced optical frequency comb, *Science* **326**, 681 (2009).
- [5] Y. Akahane, T. Asano, B.-S. Song, and S. Noda, High-Q photonic nanocavity in a two-dimensional photonic crystal, *Nature* **425**, 944 (2003).
- [6] K. J. Vahala, Optical microcavities, *Nature* **424**, 839 (2003).
- [7] A. B. Matsko and V. S. Ilchenko, Optical resonators with whispering gallery modes i: Basics, *IEEE J. Sel. Top. Quantum Electron* **12**, 3 (2006).
- [8] D. V. Strekalov, C. Marquardt, A. B. Matsko, H. G. Schwefel, and G. Leuchs, Nonlinear and quantum optics with whispering gallery resonators, *J. Opt.* **18**, 123002 (2016).
- [9] G. Lin, A. Coillet, and Y. K. Chembo, Nonlinear photonics with high-Q whispering-gallery-mode resonators, *Adv. Opt. Photon.* **9**, 828 (2017).
- [10] B. Min, T. J. Kippenberg, and K. J. Vahala, Compact, fiber-compatible, cascaded raman laser, *Opt. Lett.* **28**, 1507 (2003).
- [11] P. Latawiec, V. Venkataraman, M. J. Burek, B. J. Hausmann, I. Bulu, and M. Loncar, On-chip diamond raman laser, *Optica* **2**, 924-928 (2015).
- [12] M. Saba, C. Ciuti, J. Bloch, V. Thierry-Mieg, R. Andr e, L. S. Dang, S. Kundermann, A. Mura, G. Bongiovanni, J. Staehli, and B. Deveaud, High-temperature ultrafast polariton parametric amplification in semiconductor microcavities, *Nature* **414**, 731 (2001).
- [13] A. Dutt, K. Luke, S. Manipatruni, A. L. Gaeta, P. Nussenzeig, and M. Lipson, On-chip optical squeezing, *Phys. Rev. Appl* **3**, 044005 (2015).
- [14] A. Dutt, S. Miller, K. Luke, J. Cardenas, A. L. Gaeta, P. Nussenzeig, and M. Lipson, Tunable squeezing using coupled ring resonators on a silicon nitride chip, *Opt. Lett.* **41**, 223 (2016).
- [15] P. DelHaye, A. Schliesser, O. Arcizet, T. Wilken, R. Holzwarth, and T. Kippenberg, Optical frequency comb generation from a monolithic microresonator, *Nature* **450**, 1214 (2007).
- [16] T. J. Kippenberg, R. Holzwarth, and S. Diddams, Microresonator-based optical frequency combs, *Science* **332**, 555 (2011).
- [17] H. Jung, R. Stoll, X. Guo, D. Fischer, and H. X. Tang, Green, Red, and IR frequency comb line generation from single ir pump in an microring resonator, *Optica* **1**, 396 (2014).
- [18] T. Herr, V. Brasch, J. Jost, C. Wang, N. Kondratiev, M. Gorodetsky, and T. Kippenberg, Temporal solitons in optical microresonators, *Nat. Photonics* **8**, 145 (2014).
- [19] S.-W. Huang, H. Zhou, J. Yang, J. McMillan, A. Matsko, M. Yu, D.-L. Kwong, L. Maleki, and C. Wong, Mode-locked ultrashort pulse generation from on-chip normal dispersion microresonators, *Phys. Rev. Lett.* **114**, 053901 (2015).
- [20] Y. K. Chembo, Quantum dynamics of kerr optical frequency combs below and above threshold: Spontaneous four-wave mixing, entanglement, and squeezed states of light, *Phys. Rev. A* **93**, 033820 (2016).
- [21] S. Clemmen, K. P. Huy, W. Bogaerts, R. G. Baets, P. Emplit, and S. Massar, Continuous wave photon pair generation in silicon-on-insulator waveguides and ring resonators, *Opt. Express* **17**, 16558 (2009).
- [22] Y. Guo, W. Zhang, S. Dong, Y. Huang, and J. Peng, Telecom-band degenerate-frequency photon pair generation in silicon microring cavities, *Opt. Lett.* **39**, 2526 (2014).
- [23] D. Grassani, S. Azzini, M. Liscidini, M. Galli, M. J. Strain, M. Sorel, J. Sipe, and D. Bajoni, Micrometer-scale integrated silicon source of time-energy entangled photons, *Optica* **2**, 88 (2015).
- [24] J. W. Silverstone, R. Santagati, D. Bonneau, M. J. Strain, M. Sorel, J. L. O' Brien, and M. G. Thompson, Qubit entanglement between ring-resonator photon-pair sources on a silicon chip, *Nat. Commun.* **6** (2015).
- [25] X. Guo, C. L. Zou, C. Schuck, H. Jung, R. Cheng, and H. X. Tang, Parametric down-conversion photon-pair source on a nanophotonic chip, *Light: Science & Applications* **6**, e16249 (2017).
- [26] X. Guo, C. L. Zou, H. Jung, and H. X. Tang, On-Chip Strong Coupling and Efficient Frequency Conversion between Telecom and Visible Optical Modes, *Phys. Rev. Lett.* **117**, 123902 (2016).
- [27] Q. Li, M. Davanço, and K. Srinivasan, Efficient and low-noise single-photon-level frequency conversion interfaces using silicon nanophotonics, *Nat. Photonics* **10**, 406 (2016).
- [28] A. Rueda, F. Sedlmeir, M. C. Collodo, U. Vogl, B. Stiller, G. Schunk, D. V. Strekalov, C. Marquardt, J. M. Fink, O. Painter, G. Leuchs, and H. G. L. Schwefel, Efficient microwave to optical photon conversion: an electro-optical realization, *Optica* **3**, 597 (2016).
- [29] T. Carmon and K. J. Vahala, Visible continuous emission from a silica microphotonic device by third-harmonic generation, *Nat. Phys.* **3**, 430 (2007).

- [30] Z. Yang, P. Chak, A. D. Bristow, H. M. van Driel, R. Iyer, J. S. Aitchison, A. L. Smirl, and J. Sipe, Enhanced second-harmonic generation in AlGaAs microring resonators, *Opt. Lett.* **32**, 826 (2007).
- [31] K. Rivoire, Z. Lin, F. Hatami, W. T. Masselink, and J. Vučković, Second harmonic generation in gallium phosphide photonic crystal nanocavities with ultralow continuous wave pump power, *Opt. Express* **17**, 22609 (2009).
- [32] J. S. Levy, M. A. Foster, A. L. Gaeta, and M. Lipson, Harmonic generation in silicon nitride ring resonators, *Opt. Express* **19**, 11415 (2011).
- [33] W. Pernice, C. Xiong, C. Schuck, and H. Tang, Second harmonic generation in phase matched aluminum nitride waveguides and micro-ring resonators, *Appl. Phys. Lett.* **100**, 223501 (2012).
- [34] P. S. Kuo, J. Bravo-Abad, and G. S. Solomon, Second-harmonic generation using  $\pi$ -quasi-phasematching in a GaAs whispering-gallery-mode microcavity, *Nat. Commun.* **5** 3109 (2014).
- [35] X. Guo, C. Zou, and H. Tang, Second-harmonic generation in aluminum nitride microrings with 2500 %/ W conversion efficiency, *Optica* **3**, 1126 (2016).
- [36] Z. Lin, X. Liang, M. Lončar, S. G. Johnson, and A. W. Rodriguez, Cavity-enhanced second-harmonic generation via nonlinear-overlap optimization, *Optica* **3**, 233 (2016).
- [37] J. Moore, M. Tomes, T. Carmon, and M. Jarrahi, Continuous-wave ultraviolet emission through fourth-harmonic generation in a whispering-gallery resonator, *Opt. Express* **19**, 24139 (2011).
- [38] R. Wolf, I. Breunig, H. Zappe, and K. Buse, Cascaded second-order optical nonlinearities in on-chip micro rings, *Opt. Express* **25**, 29927 (2017).
- [39] S. Liu, Y. Zheng, and X. Chen, Cascading second-order nonlinear processes in a lithium niobate-on-insulator microdisk, *Opt. Lett.* **42**, 3626 (2017).
- [40] M. A. Marte, Competing nonlinearities, *Phys. Rev. A* **49**, 3166 (1994).
- [41] A. White, P. Lam, M. Taubman, M. Marte, S. Schiller, D. E. McClelland, and H.-A. Bachor, Classical and quantum signatures of competing  $\chi^{(2)}$  nonlinearities, *Phys. Rev. A* **55**, 4511 (1997).
- [42] K. Sasagawa and M. Tsuchiya, Highly efficient third harmonic generation in a periodically poled  $MgO : LiNbO_3$  disk resonator, *Appl. Phys Express* **2** (2009).
- [43] H. T. Tan and H. Huang, Bright quadripartite entanglement from competing  $\chi^{(2)}$  nonlinearities, *Phys. Rev. A* **83**, 1 (2011).
- [44] Z. J. Wu, Y. Ming, F. Xu, and Y. Q. Lu, Optical frequency comb generation through quasi-phase matched quadratic frequency conversion in a micro-ring resonator, *Opt. Express* **20**, 17192 (2012).
- [45] V. Ulvila, C. Phillips, L. Halonen, and M. Vainio, Frequency comb generation by a continuous-wave-pumped optical parametric oscillator based on cascading quadratic nonlinearities, *Opt. Lett.* **38**, 4281 (2013).
- [46] I. Ricciardi, S. Mosca, M. Parisi, P. Maddaloni, L. Santamaria, P. De Natale, and M. De Rosa, Frequency comb generation in quadratic nonlinear media, *Phys. Rev. A* **91**, 063839 (2015).
- [47] X. Guo and C. X. Zou, H. Jung, Z. Gong, A. Bruch, L. Jiang, and H. X. Tang, Efficient visible frequency comb generation via Cherenkov radiation from a Kerr microcomb, arXiv preprint arXiv:1704.04264 (2017).
- [48] R. W. Boyd, *Nonlinear optics* (Academic press 2003).
- [49] B. Gayral, J. Gérard, A. Lemaître, C. Dupuis, L. Manin, and J. Pelouard, High-Q wet-etched GaAs microdisks containing InAs quantum boxes, *Appl. Phys. Lett.* **75**, 1908 (1999).
- [50] A. W. Bruch, C. Xiong, B. Leung, M. Poot, J. Han, and H. X. Tang, Broadband nanophotonic waveguides and resonators based on epitaxial gan thin films, *Appl. Phys. Lett.* **107**, 141113 (2015).
- [51] C. Wang, M. J. Burek, Z. Lin, H. A. Atikian, V. Venkataraman, I.-C. Huang, P. Stark, and M. Lončar, Integrated high quality factor lithium niobate microdisk resonators, *Opt. Express* **22**, 30924 (2014).
- [52] J. Lin, Y. Xu, Z. Fang, M. Wang, J. Song, N. Wang, L. Qiao, W. Fang, and Y. Cheng, Fabrication of high-q lithium niobate microresonators using femtosecond laser micromachining, *Sci. Rep.* **5**, 8072 (2015).
- [53] A. Yariv and W. Louisell, Theory of the optical parametric oscillator, *IEEE J. Quantum. Electron.* **2**, 418 (1966).